JOURNAL OF MAGNETIC RESONANCE **124,** 393–399 (1997)
ARTICLE NO. MN961039

Measurement of Transverse Relaxation Times and Content Ratio of ^{23}Na in Phantoms Simulating Biological Systems by Use of Multiple-Quantum Filtering

K. J. JUNG,* P. J. CANNON,* AND J. KATZ*,†

*Department of Medicine (Division of Cardiology), and †Department of Radiology, College of Physicians and Surgeons, Columbia University, 630 West 168th Street, New York, NY 10032

Received September 25, 1996; revised October 14, 1996

Sodium in most biological systems relaxes biexponentially and generates a multiple-quantum signal. In a multiple-quantum filtering sequence, the sodium contributing to the multiple-quantum signal is in single-quantum coherences during the preparation and acquisition times, while it is in multiple-quantum coherences during the evolution time. In contrast to the biexponential relaxation of single-quantum coherences, double- and triple-quantum coherences relax monoexponentially during the evolution time with fast and slow transverse relaxation rates, respectively. This unique feature of multiple-quantum filtering is exploited to measure the transverse relaxation rates of phantoms simulating intracellular and extracellular sodium by analyzing the double- and triple-quantum signals acquired at various evolution times. As a byproduct, the relative ratio of multiple-quantum signals derived from intracellular and extracellular sodium can also be simultaneously determined. This technique may enable the distinction between intracellular and extracellular sodium content in biological systems without using potentially toxic shift reagents. © 1997 Academic Press

INTRODUCTION

Sodium is an important nucleus to be studied in biological systems in view of its physiological significance and good NMR sensitivity. Considerable study has been devoted to the possible distinction between intracellular and extracellular sodium in biological systems without using shift reagents to discriminate between them (*1*). In an early stage, techniques to distinguish between intracellular and extracellular sodium were based on the assumption that the transverse relaxation rate of intracellular sodium was faster than that of extracellular sodium (*2*). On the other hand, ever since it was first reported that only intracellular sodium generated a multiple-quantum (MQ) signal (*3*), a great deal of attention has been devoted to the application of MQ filtering to the study of sodium in biological systems.

However, recent studies with the aid of shift reagents such as $Dy(PPP)_2^{7-}$, $DyTTHA^{3-}$, and $TmDOTP^{5-}$ have shown that both intracellular and extracellular sodium relax biexponentially with fast (R_{2f}^{in} and R_{2f}^{ex}) and slow (R_{2s}^{in} and R_{2s}^{ex}) transverse relaxation rates, respectively (*4–7*). Thus, both intracellular and extracellular sodium can generate MQ signals through biexponential relaxation, and consequently, shift reagents are still needed in MQ filtering to distinguish between intracellular and extracellular sodium (*6–8*). Unfortunately, shift reagents are potentially toxic and, in general, themselves alter the relaxation rates. Therefore, a technique has been sought to distinguish between intracellular and extracellular sodium without using shift reagents (*4, 9*).

We here exploit the unique characteristics of MQ sodium signals to develop a technique which can permit the measurement of the transverse relaxation rates for both intracellular and extracellular sodium without the need of shift reagents (*10, 11*). We also demonstrate that with these measurements it is possible to determine the relative ratio of the intracellular and extracellular sodium generating MQ signals.

METHODS

The MQ pulse sequence with refocused preparation (τ_P) and evolution (τ_E) times may be represented as

$$(\theta_1, \phi_1)\text{—}\frac{\tau_P}{2}\text{—}(\theta_2, \phi_2)\text{—}\frac{\tau_P}{2}\text{—}(\theta_3, \phi_3)$$
$$\text{—}\frac{\tau_E}{2}\text{—}(\theta_4, \phi_4)\text{—}\frac{\tau_E}{2}\text{—}(\theta_5, \phi_5)\text{—}Acq(t_2, \phi_R), \qquad [1]$$

where ϕ_n denotes the phase of each RF pulse with flip angle θ_n, ϕ_R is the receiver phase, and t_2 is the acquisition time. In general, the flip angles of the first and refocusing RF pulses are set to $\pi/2$ and π, respectively, i.e., $\theta_1 = \pi/2$ and $\theta_2 = \theta_4 = \pi$.

During the preparation and acquisition times, the single-quantum (SQ) coherence contributing to MQ signals relaxes biexponentially with fast (R_{2f}) and slow (R_{2s}) transverse

1090-7807/97 $25.00

relaxation rates, where $R_{2f} > R_{2s}$. This may be represented by SQ rank-conversion functions $f_{l'l}^{(1)}$, defined as

$$f_{31}^{(1)}(\tau_P) = \frac{\sqrt{6}}{5}[\exp(-R_{2f}\tau_P) - \exp(-R_{2s}\tau_P)] \quad [2]$$

and

$$f_{13}^{(1)}(t_2) = \frac{\sqrt{6}}{5}[\exp(-R_{2f}^* t_2) - \exp(-R_{2s}^* t_2)], \quad [3]$$

where l and l' denote the initial and converted ranks of the tensors, respectively (*12, 13*). For simplicity, we will focus on the third-rank MQ signal, i.e., $l = 3$, but a similar argument may be presented for the second-rank MQ signal (*14*). In Eq. [3], R_{2f}^* and R_{2s}^* denote the corresponding relaxation rates affected by magnetic field inhomogeneity. Note that the terms involving the fast and slow relaxation rates in Eq. [2] are opposite in their polarities, making MQ filtering better than the conventional SQ technique in the calculation of biexponential relaxation rates by curve fitting (cf. Eq. [21]) (*7, 15*).

In contrast to the biexponential relaxation of the SQ coherence, both double- (DQ) and triple-quantum (TQ) coherences relax monoexponentially during the evolution time, with transverse relaxation rates R_{2f} and R_{2s}, respectively. This may be represented by MQ rank-conversion functions $f_{33}^{(m)}$, where

$$f_{33}^{(2)}(\tau_E) = \exp(-R_{2f}\tau_E) \quad [4]$$

and

$$f_{33}^{(3)}(\tau_E) = \exp(-R_{2s}\tau_E) \quad [5]$$

for DQ and TQ coherences, respectively (*16*). In other words, the biexponential relaxation of the SQ coherence can be inherently decomposed into two MQ monoexponential relaxation components during the evolution time.

Then, the spectral peak amplitudes of acquired DQ and TQ signals, i.e., S_{32} and S_{33}, may be described as

$$S_{3m}(\tau_E) = a_{3m}M f_{31}^{(1)}(\tau_P)(T_{2f}^* - T_{2s}^*) f_{33}^{(m)}(\tau_E), \quad [6]$$

where M denotes the equilibrium sodium magnetization generating an MQ signal through biexponential relaxation; T_{2f} and T_{2s} are the fast and slow transverse relaxation times (reciprocals of R_{2f} and R_{2s}, respectively); T_{2f}^* and T_{2s}^* represent the corresponding relaxation times affected by magnetic field inhomogeneity; and a_{3m} incorporates all the remaining factors (14). Upon further defining

$$b_{3m}(\tau_P) = a_{3m}M f_{31}^{(1)}(\tau_P)(T_{2f}^* - T_{2s}^*), \quad [7]$$

Eq. [6] may be simplified as

$$S_{3m}(\tau_E) = b_{3m}(\tau_P) f_{33}^{(m)}(\tau_E). \quad [8]$$

As previously mentioned, both intracellular and extracellular sodium in biological systems relax biexponentially. In what follows, we shall denote the intracellular and extracellular components by superscripts in and ex, respectively. Then, the MQ spectral peak amplitudes of intracellular and extracellular sodium may be expressed from Eq. [8] as

$$S_{3m}^{in}(\tau_E) = b_{3m}^{in}(\tau_P) f_{33}^{(m)in}(\tau_E) \quad [9]$$

and

$$S_{3m}^{ex}(\tau_E) = b_{3m}^{ex}(\tau_P) f_{33}^{(m)ex}(\tau_E), \quad [10]$$

respectively.

The total MQ spectral peak amplitude derived from the third-rank m-quantum tensors during the evolution time may be described as a linear superposition of the intracellular and extracellular MQ spectral peak amplitudes, i.e.,

$$S_{3m}^{tot}(\tau_E) = S_{3m}^{in}(\tau_E) + S_{3m}^{ex}(\tau_E). \quad [11]$$

By use of Eqs. [9] to [11], the total DQ and TQ spectral peak amplitudes may be expressed as

$$S_{32}^{tot}(\tau_E) = b_{32}^{ex}(\tau_P)[\rho(\tau_P) f_{33}^{(2)in}(\tau_E) + f_{33}^{(2)ex}(\tau_E)] \quad [12]$$

and

$$S_{33}^{tot}(\tau_E) = b_{33}^{ex}(\tau_P)[\rho(\tau_P) f_{33}^{(3)in}(\tau_E) + f_{33}^{(3)ex}(\tau_E)], \quad [13]$$

respectively, where

$$\rho(\tau_P) = \frac{b_{3m}^{in}(\tau_P)}{b_{3m}^{ex}(\tau_P)} = \frac{M^{in}}{M^{ex}} \frac{f_{31}^{(1)in}(\tau_P)}{f_{31}^{(1)ex}(\tau_P)} \frac{(T_{2f}^{in*} - T_{2s}^{in*})}{(T_{2f}^{ex*} - T_{2s}^{ex*})}. \quad [14]$$

Note that $\rho(\tau_P)$ is independent of the coherence order and the evolution time.

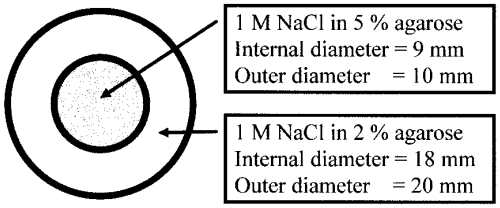

FIG. 1. A cross section of the composite phantom consisted of two coaxial NMR tubes.

In general, the intracellular relaxation rates are larger than the corresponding extracellular relaxation rates, i.e., (7)

$$r_f = \frac{R_{2f}^{in}}{R_{2f}^{ex}} > 1 \qquad [15]$$

and

$$r_s = \frac{R_{2s}^{in}}{R_{2s}^{ex}} > 1. \qquad [16]$$

Therefore, if MQ signals are acquired at several different evolution times, the relaxation rates can be calculated by curve fitting based on Eqs. [12] and [13].

Furthermore, Eq. [14] may be rearranged to obtain the ratio M^{in}/M^{ex} as

$$\frac{M^{in}}{M^{ex}} = \rho(\tau_P)\,\frac{f_{31}^{(1)ex}(\tau_P)}{f_{31}^{(1)in}(\tau_P)}\,\frac{(T_{2f}^{ex}* - T_{2s}^{ex}*)}{(T_{2f}^{in}* - T_{2s}^{in}*)}. \qquad [17]$$

Therefore, once the magnetic field inhomogeneity is determined, the sodium content ratio M^{in}/M^{ex} can be estimated from the relaxation times and the ratio $\rho(\tau_P)$ obtained as a byproduct of the calculation of the relaxation rates from Eq. [12].

EXPERIMENTAL RESULTS

In vivo MQ signals are generated from intracellular and extracellular sodium, interacting with proteins. Because sodium in a gel such as agarose can generate an MQ signal through biexponential relaxation (*17*) and because the concentration of agarose affects the relaxation rates (*18*), the behavior of intracellular and extracellular sodium can be mimicked by phantoms containing sodium in 5 and 2% agarose (w/v, Sigma A-9539), respectively. Two different types of phantoms, i.e., two individual and one composite phantoms, were constructed. The two individual phantoms consisted of a 20 mm NMR tube containing 1 *M* NaCl in either 5 or 2% agarose so that each phantom had one set of biexponential relaxation rates. The composite phantom (Fig. 1) consisted of two coaxial NMR tubes containing 1 *M* NaCl in 5 and 2% agarose to simulate extracellular sodium surrounding intracellular sodium so that the phantom had two sets of biexponential relaxation rates as for sodium in biological systems.

The NMR system was a Bruker AM-300 (7.05 T) with the carrier frequency set to the on-resonance frequency (=79.58 MHz) throughout the experiments (*19*). The pulse sequence [1] was used with $\theta_3 = \theta_5 = \frac{1}{4}\pi$ for DQ filtering and $\theta_3 = \theta_5 = \frac{1}{2}\pi$ for TQ filtering. The phase-cycling schemes employed for DQ and TQ filtering are listed in Tables 1 and 2, respectively (*14, 19*). The DQ filtering scheme [scheme 4 in Ref. (*14*)] was chosen in order to maintain the same functional dependence on the RF flip angle as for TQ filtering (*14*). The preparation time was set to 8 ms to maximize the MQ sodium signal for 5% agarose. The pulse repetition time was 500 ms which was long enough to avoid saturation and occurrence of the intersequence stimulated echo (*20, 21*). The number of DQ and TQ acquisitions were 256 and 144, respectively. In order to follow the relaxation faithfully, the number of evolution time samplings was greater than the required minimum, which is 2 for the individual phantoms and 4 for the composite phantom. The temperature was 19°C. In performing Fourier transform of the acquired time data, no line broadening was employed. The computer program for curve fitting was a DeltaGraph Pro 3.5 for Win 3.1.

First, DQ and TQ signals were acquired from each of the two individual phantoms at several evolution times. The biexponential relaxation rates of each phantom were calculated by fitting the spectral peak amplitudes to Eqs. [9] and [10] (Figs. 2 and 3) and are summarized in Table 3.

Second, DQ and TQ signals were acquired from the composite phantom. Exploiting the fact that r_f (=2.2) > r_s (=1.3) as found from the individual phantoms, R_{2f}^{in} and R_{2f}^{ex} were calculated by fitting the DQ spectral peak amplitudes to Eq. [12]. This curve fitting also yielded the ratio $\rho(\tau_P)$ (=0.52), which was then used as a constraint in calculating R_{2s}^{in} and R_{2s}^{ex} by fitting the TQ spectral peak amplitudes to Eq. [13] (Fig. 4). The goodness of the curve fitting is demonstrated by decomposing the DQ and TQ spectral peak amplitudes into fast- and slow-relaxation components according to Eqs. [12] and [13] by use of the measured relaxation rates and $\rho(\tau_P)$ (Figs. 5A and 5B, respectively). The measured relaxation times are summarized in Table 3.

Finally, the sodium content ratio M^{in}/M^{ex} was estimated from Eq. [17], followed by the measurement of the magnetic field inhomogeneity. If $\Delta\nu$ denotes the linewidth measured from the SQ FID signal, $\Delta\nu_{B_0}$ the linewidth due to magnetic field inhomogeneity, and $\Delta\nu_{T_2}$ the linewidth due to the transverse relaxation, then the following relation holds:

$$\Delta\nu = \Delta\nu_{B_0} + \Delta\nu_{T_2}. \qquad [18]$$

TABLE 1
Phase-Cycling Scheme for DQ Filtering

Phase	Phase list (×90°)
ϕ_1	0 1 2 3 0 3 2 1 2 3 0 1 2 1 0 3
ϕ_2	0 1 2 3 0 3 2 1 0 1 2 3 0 3 2 1 1 2 3 0 1 0 3 2 1 2 3 0 1 0 3 2 2 3 0 1 2 1 0 3 2 3 0 1 2 1 0 3 3 0 1 2 3 2 1 0 3 0 1 2 3 2 1 0
ϕ_3	1 2 3 0 1 0 3 2
ϕ_4	0 0 0 0 0 0 0 0 0 0 0 0 0 0 0 0 0 0 0 0 0 0 0 0 0 0 0 0 0 0 0 0 2 2 2 2 2 2 2 2 2 2 2 2 2 2 2 2 2 2 2 2 2 2 2 2 2 2 2 2 2 2 2 2 4 4 4 4 4 4 4 4 4 4 4 4 4 4 4 4 4 4 4 4 4 4 4 4 4 4 4 4 4 4 4 4 6 6 6 6 6 6 6 6 6 6 6 6 6 6 6 6 6 6 6 6 6 6 6 6 6 6 6 6 6 6 6 6
ϕ_5	1
ϕ_R	0 2 0 2 0 2 0 2 2 0 2 0 2 0 2 0 2 0 2 0 2 0 2 0 0 2 0 2 0 2 0 2

Therefore, to determine $\Delta\nu_{B_0}$, $\Delta\nu_{T_2}$ must be calculated first. In the case of multiexponential relaxation, $\Delta\nu_{T_2}$ cannot be calculated unless all the relaxation times are known. A conventional approach is to simplify the multiexponential relaxation to monoexponential relaxation by acquiring the SQ FID signal contributed solely from the slowest-relaxation component, i.e., R_{2s}^{ex} (*22*). This approach is also feasible in this case, but this would yield $\Delta\nu_{B_0}$ only for the extracellular space, i.e., the outer cylinder of the composite phantom. Thus, we instead measured $\Delta\nu_{B_0}$ for both intracellular and extracellular spaces by use of the relaxation rates measured by the technique proposed here and the geometry of the composite phantom.

The absorptive Lorenzian spectrum for the SQ FID with transverse relaxation time T_2 is given by

$$g(T_2, \nu) = \frac{T_2}{1 + (2\pi\nu T_2)^2}, \qquad [19]$$

where ν denotes an off-resonance frequency (*23*). For the spectrum in Eq. [19], the linewidth $\Delta\nu_{T_2}$ is given as

$$\Delta\nu_{T_2} = \frac{1}{\pi T_2}. \qquad [20]$$

On the other hand, the SQ signal from the nuclei with biexponential relaxation may be described by

$$S_{11}(t_2) = a_{31}M[0.6\exp(-R_{2f}t_2) + 0.4\exp(-R_{2s}t_2)], \qquad [21]$$

where a_{31} is a constant (*12, 13*). Therefore, the absorptive Lorenzian spectra for intracellular and extracellular spaces may be described as a linear superposition of the Lorenzian spectra for the corresponding fast- and slow-relaxation components as

$$g^{in}(\nu) = 0.6g(T_{2f}^{in}, \nu) + 0.4g(T_{2s}^{in}, \nu) \qquad [22]$$

and

$$g^{ex}(\nu) = 0.6g(T_{2f}^{ex}, \nu) + 0.4g(T_{2s}^{ex}, \nu), \qquad [23]$$

respectively. Then, the absorptive Lorenzian spectrum $g^{tot}(\nu)$ for the total space can be expressed as

TABLE 2
Phase-Cycling Scheme for TQ Filtering

Phase	Phase list (×30°)
ϕ_1	0 2 4 6 8 10 6 8 10 0 2 4
ϕ_2	0 2 4 6 8 10 0 2 4 6 8 10 3 5 7 9 11 1 3 5 7 9 11 1 6 8 10 0 2 4 6 8 10 0 2 4 9 11 1 3 5 7 9 11 1 3 5 7
ϕ_3	3 5 7 9 11 1
ϕ_4	0 0 0 0 0 0 0 0 0 0 0 0 2 2 2 2 2 2 2 2 2 2 2 2 4 4 4 4 4 4 4 4 4 4 4 4 6 6 6 6 6 6 6 6 6 6 6 6 8 8 8 8 8 8 8 8 8 8 8 8 10 10 10 10 10 10 10 10 10 10 10 10
ϕ_5	3
ϕ_R	0 6 0 6 0 6 6 0 6 0 6 0 6 0 6 0 6 0 0 6 0 6 0 6

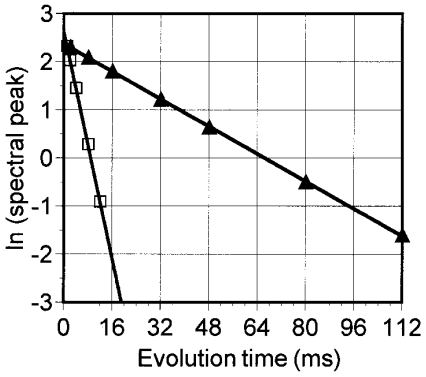

FIG. 2. DQ (□) and TQ (▲) spectral peak amplitudes at various evolution times acquired from a phantom containing NaCl in 5% agarose. DQ and TQ spectral peak amplitudes are normalized by setting the maximum peak amplitudes to 10 and then converted into a natural logarithm (*ln*) scale. The fitting lines are overlaid. Values of χ^2 for DQ and TQ spectral peak amplitudes were 2.1×10^{-4} and 1.3×10^{-3}, respectively.

$$g^{\text{tot}}(\nu) = \frac{M^{\text{ex}}}{M^{\text{in}} + M^{\text{ex}}} \left[\frac{M^{\text{in}}}{M^{\text{ex}}} g^{\text{in}}(\nu) + g^{\text{ex}}(\nu) \right]. \quad [24]$$

On the other hand, the actual $M^{\text{in}}/M^{\text{ex}}$ can be calculated from the geometry of the composite phantom shown in Fig. 1. Since the sodium concentrations in the two coaxial tubes of the composite phantom are the same, the actual $M^{\text{in}}/M^{\text{ex}}$ can be determined from the corresponding volumes V^{in} and V^{ex}, i.e.,

$$\text{actual } \frac{M^{\text{in}}}{M^{\text{ex}}} = \frac{V^{\text{in}}}{V^{\text{ex}}} = 0.36. \quad [25]$$

Equation [25] holds as written, provided that the proportion of the sodium content with biexponential relaxation vs the total sodium content is the same for the sodium in 5 and 2% agarose (*24, 25*). Then, Eq. [24] can be rewritten by use of Eq. [25] as

$$g^{\text{tot}}(\nu) = \frac{V^{\text{ex}}}{V^{\text{in}} + V^{\text{ex}}} \left[\frac{V^{\text{in}}}{V^{\text{ex}}} g^{\text{in}}(\nu) + g^{\text{ex}}(\nu) \right]. \quad [26]$$

Equation [26] was calculated for the measured relaxation rates and the volume ratio of the composite phantom. From the resultant plot shown in Fig. 6, $\Delta\nu_{T_2}$ was estimated as 13 Hz. On the other hand, $\Delta\nu$ was measured from the SQ FID as 22 Hz (Fig. 6). Substitution of the estimated $\Delta\nu_{T_2}$ and the experimentally measured $\Delta\nu$ into Eq. [18] yields $\Delta\nu_{B_0} = 9$ Hz. For comparison, $\Delta\nu_{B_0}$ (=8 Hz) was also measured from the SQ FID acquired after the spin-echo time of 120 ms ($>4 \times T_{2s}^{\text{in}}$). As discussed above, such a measurement represents $\Delta\nu_{B_0}$ only for the outer cylinder of the composite phantom. For biological systems, however, this conventional technique may be employed since the intracellular and extracellular spaces are finely interwoven.

TABLE 3
Measured Transverse Relaxation Times in Units of ms

	5% agarose		2% agarose	
	T_{2f}^{in}	T_{2s}^{in}	T_{2f}^{ex}	T_{2s}^{ex}
Individual phantoms	3.4	28	7.5	37
Composite phantom	3.2	26	7.5	38

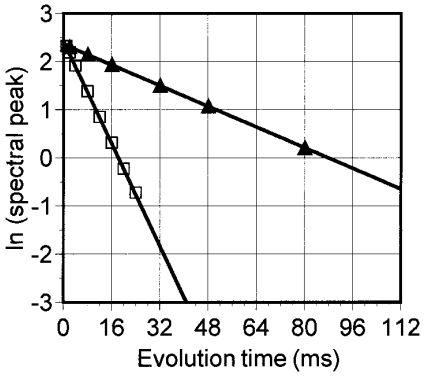

FIG. 3. DQ (□) and TQ (▲) spectral peak amplitudes at various evolution times acquired from a phantom containing NaCl in 2% agarose. DQ and TQ spectral peak amplitudes are normalized by setting the maximum peak amplitudes to 10 and then converted into a natural logarithm (*ln*) scale. The fitting lines are overlaid. Values of χ^2 for DQ and TQ spectral peak amplitudes were 9.3×10^{-4} and 1.6×10^{-5}, respectively.

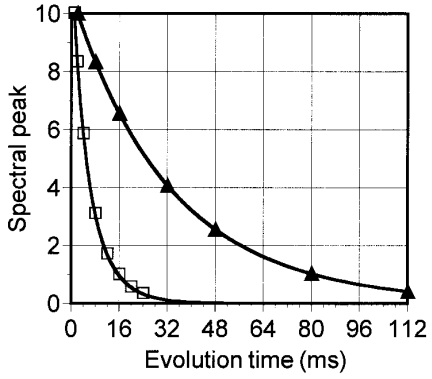

FIG. 4. DQ (□) and TQ (▲) spectral peak amplitudes at various evolution times acquired from the composite phantom in Fig. 1. DQ and TQ spectral peak amplitudes are normalized by setting the maximum peak amplitudes to 10. Values of χ^2 for DQ and TQ spectral peak amplitudes were 8.9×10^{-4} and 3.1×10^{-4}, respectively. The fitting functions for DQ and TQ were $y = 8.0\ [\mathbf{0.52}\ \exp(-x/\mathbf{3.2}) + \exp(-x/\mathbf{7.5})]$ and $y = 7.0[0.52\ \exp(-x/\mathbf{26}) + \exp(-x/\mathbf{38})]$, respectively, with major parameters typed in bold.

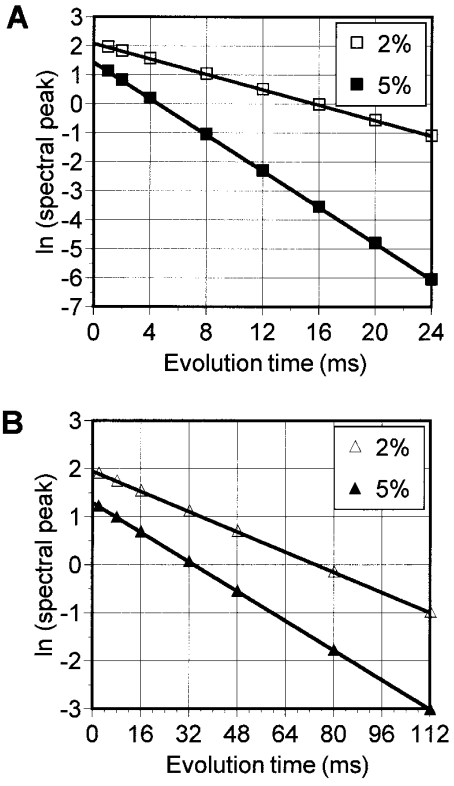

FIG. 5. Decomposition of the DQ (A) and TQ (B) spectra in Fig. 4 into two relaxation components, respectively. The decomposed spectral peak amplitudes are linear on a natural logarithm scale, confirming that the decomposed spectral peak amplitudes are monoexponential, i.e., the fast- and slow-relaxation components are from the sodium in the 5 and 2% agarose systems, respectively.

Using the relation

$$T_2^* = \frac{T_2}{1 + \pi\Delta\nu_{B_0}T_2}, \qquad [27]$$

the ratio M^{in}/M^{ex} can now be estimated from Eq. [17] as

$$\frac{M^{in}}{M^{ex}} = 0.52\,\frac{[\exp(-8/7.5) - \exp(-8/38)]}{[\exp(-8/3.2) - \exp(-8/26)]}\,\frac{(6.2 - 18.3)}{(2.9 - 15.0)} = 0.37. \qquad [28]$$

Considering the potential difference of RF flip angles and magnetic field inhomogeneity between the inner and outer cylinders of the composite phantom, this result is quite close to the actual value. In actual biological systems, the intracellular and extracellular spaces are so finely interwoven that the average RF flip angles and magnetic field inhomogeneity would be the same for both spaces.

Even though the relaxation times measured from the composite phantom agree well with those measured from the individual phantoms, the curve fitting would be improved even further with better conditions for r_f, r_s, and $\rho(\tau_P)$, as in fact they occur in biological systems. To see the effect of the minor discrepancy between the measured relaxation times of the composite phantom and those measured from the individual phantoms, the DQ spectral peaks of the composite phantom were fitted with the relaxation times measured from the individual phantoms. This fitting resulted in increases of χ^2 (from 8.9×10^{-4} to 2.2×10^{-3}) and $\rho(\tau_P)$ (from 0.52 to 0.56), but the fitted curve was still close to the experimental data. For the new $\rho(\tau_P)$ (=0.56), the relaxation times T_{2s}^{in} and T_{2s}^{ex} calculated by Eq. [13] were unchanged. Furthermore, the substitution of these new values into Eq. [17] resulted in the same value for M^{in}/M^{ex} as that obtained in Eq. [28].

CONCLUSIONS

It is confirmed in phantoms that DQ and TQ signals derived from biexponentially relaxing sodium relax monoexponentially during the evolution time with fast and slow relaxation rates, respectively. This unique decomposition feature of MQ filtering has been exploited to measure two sets of biexponential transverse relaxation rates of the composite phantom simulating intracellular and extracellular sodium. By use of the measured relaxation rates, a new approach for the determination of the magnetic field inhomogeneity has also been presented. Furthermore, the relative ratio between the intracellular and extracellular sodium content has been

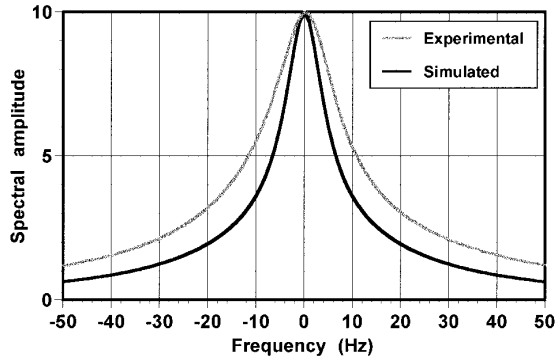

FIG. 6. SQ spectra of the composite phantom, used to determine the linewidth due to magnetic field inhomogeneity. The real part of the spectrum from an SQ FID is shown together with the simulated absorptive Lorenzian spectrum calculated from the relaxation times and the geometry of the composite phantom. From these spectra, $\Delta\nu$ = 22 Hz and $\Delta\nu_{T_2}$ = 13 Hz, respectively. Subtraction of $\Delta\nu_{T_2}$ from $\Delta\nu$ results in $\Delta\nu_{B_0}$ = 9 Hz.

obtained as a byproduct of the calculation of the relaxation rates. This may be of major importance for the physiologic study of sodium and other quadrupolar nuclei in biological systems since potentially toxic shift reagents are not employed.

ACKNOWLEDGMENTS

The authors thank Dr. Myron L. Weisfeldt for support and discussions. Thanks are also due to Dr. Daniel Burkhoff for discussions. Furthermore, the assistance of Mr. Anguo Gu and Dr. Shu-Ming Zhu in the preparation of the phantoms is also appreciated.

REFERENCES

1. P. M. Joseph, *in* ''Encyclopedia of Nuclear Magnetic Resonance'' (D. M. Grant and R. K. Harris, Eds.), p. 4445, Wiley, New York, 1996.
2. S. K. Hilal, J. B. Ra, C. H. Oh, I. K. Mun, S. G. Einstein, and P. Roschmann, *in* ''Magnetic Resonance Imaging'' (D. D. Stark and W. G. Bradley, Jr., Eds.), Chap. 31, Mosby Year Book, St. Louis, 1988.
3. J. Pekar, P. F. Renshaw, and J. S. Leigh, Jr., *J. Magn. Reson.* **72,** 159 (1987).
4. L. A. Jelicks and R. K. Gupta, *J. Magn. Reson.* **83,** 146 (1989).
5. B. D. Foy and D. Burstein, *Magn. Reson. Med.* **27,** 270 (1992).
6. L. A. Jelicks and R. K. Gupta, *Magn. Reson. Med.* **29,** 130 (1993).
7. J. M. Dizon, J. S. Tauskela, D. Wise, D. Burkhoff, P. J. Cannon, and J. Katz, *Magn. Reson. Med.* **35,** 336 (1996).
8. J. S. Tauskela, J. M. Dizon, P. J. Cannon, and J. Katz, *J. Magn. Reson. B* **108,** 165 (1995).
9. R. C. Lyon and A. C. McLaughlin, *Biophys. J.* **67,** 369 (1994).
10. K. J. Jung and J. Katz, *Exp. Nucl. Magn. Reson. Conf.,* WP 207 (1996).
11. K. J. Jung and J. Katz, *Int. Soc. Magn. Reson. Med.,* 1173 (1996).
12. G. Jaccard, S. Wimperis, and G. Bodenhausen, *J. Chem. Phys.* **85,** 6282 (1986).
13. J. R. C. van der Maarel, *Chem. Phys. Lett.* **155,** 288 (1989).
14. K. J. Jung, J. S. Tauskela, and J. Katz, *J. Magn. Reson. B* **112,** 103 (1996).
15. W. D. Rooney and C. S. Springer, Jr., *J. Magn. Reson.* **75,** 297 (1987).
16. W. D. Rooney and C. S. Springer, Jr., *NMR Biomed.* **4,** 227 (1991).
17. J. Andrasko, *J. Magn. Reson.* **16,** 502 (1974).
18. G. S. Payne and P. Styles, *J. Magn. Reson.* **95,** 253 (1991).
19. K. J. Jung and J. Katz, *J. Magn. Reson. B* **112,** 214 (1996).
20. K. J. Jung, J. Katz, L. M. Boxt, S. K. Hilal, and Z. H. Cho, *J. Magn. Reson. B* **107,** 235 (1995).
21. K. J. Jung and J. Katz, *J. Magn. Reson.* **124,** 232 (1997).
22. J. L. Allis, A. M. L. Seymour, and G. K. Radda, *J. Magn. Reson.* **93,** 71 (1991).
23. J. Cavanagh, W. J. Fairbrother, A. G. Palmer III, and N. J. Skelton, ''Protein NMR Spectroscopy Principles and Practice,'' Academic Press, San Diego, 1996.
24. R. B. Hutchison, D. Malhotra, R. E. Hedrick, L. Chan, and J. I. Shapiro, *J. Biol. Chem.* **265,** 15506 (1990).
25. J. Whang, J. Katz, L. M. Boxt, K. Reagan, D. J. Sorce, R. R. Sciacca, and P. Cannon, *J. Magn. Reson. B* **103,** 175 (1994).